CHEMOSTRATIGRAPHIC AND SEQUENCE STRATIGRAPHIC ANALYSIS OF THE AUSTIN GROUP IN THE OUTCROPS AND SUBSURFACE OF TEXAS

A Thesis

by

MOLLY ELIZABETH MCCREARY

Submitted to the Graduate and Professional School of
Texas A&M University
in partial fulfillment of the requirements for the degree of

MASTER OF SCIENCE

Chair of Committee,	Michael Pope
Co-Chair of Committee,	Arthur Donovan
Committee Member,	Franco Marcantonio
Head of Department,	Julie Newman

August 2022

Major Subject: Geology

ABSTRACT

The Austin Group, comprised of chalk and marly chalk, is a classic fractured chalk play, that has seen a renaissance as an unconventional reservoir exploited by the combination of fracking and horizontal drilling across Texas. At first glance, the Austin Group in outcrop, as well as in core, often appears as a vertically monotonous, homogenous succession of skeletal wackestones (chalk) alternating with argillaceous-prone mudstone beds. Detailed petrophysical, x- ray fluorescence (XRF) chemostratigraphic, and sequence stratigraphic analysis of the Austin Group in cores and outcrops across Texas, however, reveals a vertical succession of three chemostratigraphically-distinct, unconformity-bounded, chronostratigraphic units, which are defined and mapped in this study as the Lower, Middle, and Upper Austin Formations.

The Latest Turonian to Late Coniacian Lower Austin Formation is a carbonate-rich, clay-poor depositional sequence that was deposited unconformably above the Eagle Ford Group. The Latest Coniacian to Middle Santonian Middle Austin Formation is a more argillaceous-rich depositional sequence, containing increased amounts of aluminum, silica, and titanium. The Middle Santonian to Middle Campanian Upper Austin Formation is the most carbonate-poor and terrigenous-rich depositional sequence within the Austin Group, and a regional unconformity separates it from the overlying Taylor Group.

The carbonate-rich Lower Austin Formation is the primary unconventional reservoir target of the Fractured Austin Chalk play across Texas. A detailed study of this lower unit was conducted in outcrop exposures along U.S. Highway 90 in Val Verde County, Texas. The Lower Austin Formation also was analyzed in several industry and United States Geological Survey (USGS) research boreholes across Texas. Analysis of this core data indicates that the Lower Austin

Formation systematically becomes more terrigenous/argillaceous-rich northward towards Dallas. This facies change is interpreted to record more proximal depositional environments within the Lower Austin Formation.

ACKNOWLEDGEMENTS

To begin, I would like to thank ConocoPhillips for providing a full funding opportunity for me to study under the tutelage of Dr. Donovan and Dr. Pope at Texas A&M University. Secondly, I am grateful to the United States Geological Survey for allowing access, data, and support for the cores used in this thesis. Sincerest thanks to my advisors, for teaching me that "the wheel doesn't need to be reinvented," as well as, how to "see the forest through the trees," and many, many more necessary idioms. Without the help of Christine Griffith, my knowledge of the Austin Chalk would be a fraction of what it is today. Additionally, I would like to extend my gratitude towards Bobby Reece, Nick Perez, Juan Carlos Laya Pereira, Maria Gutierrez Azuaje, Eric Riggs, Tony Dincau, Jason Ward, Mike Unger, Sidney Dangtran, and especially Alexandra Snell and Jessica McKay, for all showing me that a career in geology isn't about a job, but rather "geologic intuition" is simply the unwavering curiosity about the Earth around you. Cameron Manche and Scott Gifford were key members to the field studies along U.S. Highway 90, and Samantha MacKenzie also assisted as a research assistant in this study.

Finally, I would like to thank Jason Kurten, Abbey Arends, and Mita Coker for keeping me sane and in the outdoors; Jordan Whittle, Grant Rogers, and the Breakfast Club for giving me a reason to stay and making it hard to leave; my JGIU friends for getting me up every morning; Caroline Eckert for turning me into a hopeful person; Sarah and the entire Escobedo clan for teaching me the most important lesson in life is to go for the blue shoe, but have fun doing it; and most of all, my family. Without their support and direction, I would be lost, but still loved. For every decision I make is to make them proud.

CONTRIBUTORS AND FUNDING SOURCES

This work was supervised by a thesis committee consisting of Professor Michael Pope and Professor Arthur Donovan of the Department of Geology and Geophysics and Professor Franco Marcantonio of the Department of Oceanography. Funding for graduate study, core access, and data was provided by the ConocoPhillips fellowship position through the Unconventional Reservoirs and Outcrop Characterization (UROC) Consortium. Access to cores was provided by the United States Geological Survey, the Bureau of Economic Geology, and the Texas Christian University Core Facility.

Scholarships used for core access and outcrop research were funded by the East Texas Communities Foundation Geoscience Scholarship, Natural Gas Society of East Texas Scholarship, Marathon Oil Scholarship, Hess Leadership Scholarship, Society of Independent & Professional Earth Scientists Scholarship, ConocoPhillips/HEEP Endowed Graduate Fellowship, and the Houston Geological Society Calvert Memorial Scholarship. All other work conducted for the thesis was completed by the student independently.

TABLE OF CONTENTS

LIST OF FIGURES

FIGURE Page

LIST OF TABLES

INTRODUCTION

The Upper Cretaceous Austin Group is a low permeability, highly fractured onshore oil and gas chalk play spanning from southwest Texas to south-central Louisiana (Ewing, 1991). The fracture system within the Austin Group is oriented sub-parallel to the Lower Cretaceous carbonate shelf edge (Kilcoyne, 2018). The movement and uplift of the Jurassic Louann Salt created an extensive fracture network in which the hydrocarbons are stored, creating fields and reservoirs updip of the shelf edge above and adjacent to salt domes. The study area of this project (Fig. 1) spans from the Maverick Basin (MB) and the Rio Grande Embayment, across the San Marcos Arch (SMA), and into the northwest part of the East Texas Basin (ETB).

Composed primarily of coccolithophores (Folk 1959), the Austin Group (Dawson, et al, 1995) is a low- permeability and -porosity skeletal wackestone (chalk). However, natural intersecting fracture systems within the Austin Chalk allows it to store and produce hydrocarbons (Friedman et al., 1995). Layers of clay-rich marl alternate with skeletal wackestones (chalk) to create a heterogeneous Austin Chalk Group with poor pore interconnectedness within the reservoir, negatively affecting production when drilling (Corbett et al., 1987).

The underlying Upper Cretaceous Eagle Ford Group provides the hydrocarbons in Austin Group reservoirs (Pearson, 2012). The Eagle Ford Group oil and gas generated during the early Miocene began vertically migrating through the microfractures of the shale and into the Austin Group through its extensive system of joints and fractures (Pearson, 2012). Accumulations of hydrocarbons within heavily fractured zones in the Austin Group historically made the Austin Chalk an ideal candidate for horizontal drilling. As depletion of the reservoir continues with an additional decline in the rate of production, combining horizontal drilling with stimulus and

fracking has led to higher recovery from this low-permeability, low-porosity formation (Dawson, et al, 1995).

Understanding the distribution of the lateral and vertical facies variations of the Austin Group across the state of Texas is of economic importance for companies interested in oil and gas recovery within this unit. Key to this study were USGS Research cores that spanned most of the Austin Chalk, and all the underlying penetrate the Eagle Ford Group. These cores, which are located in Dallas, McLellan, and Uvalde counties (Figure 1), provide a unique opportunity to conduct advanced x-ray fluorescence (XRF) analysis of the Eagle Ford Group, as well as the Lower Austin Formation across the state (Figure 1). Integrating chemostratigraphic (XRF) and petrophysical data, as well as sequence stratigraphic analysis, provides insights into the vertical and lateral elemental variability of the Austin Group, within a chronostratigraphic framework, for the first time across Texas.

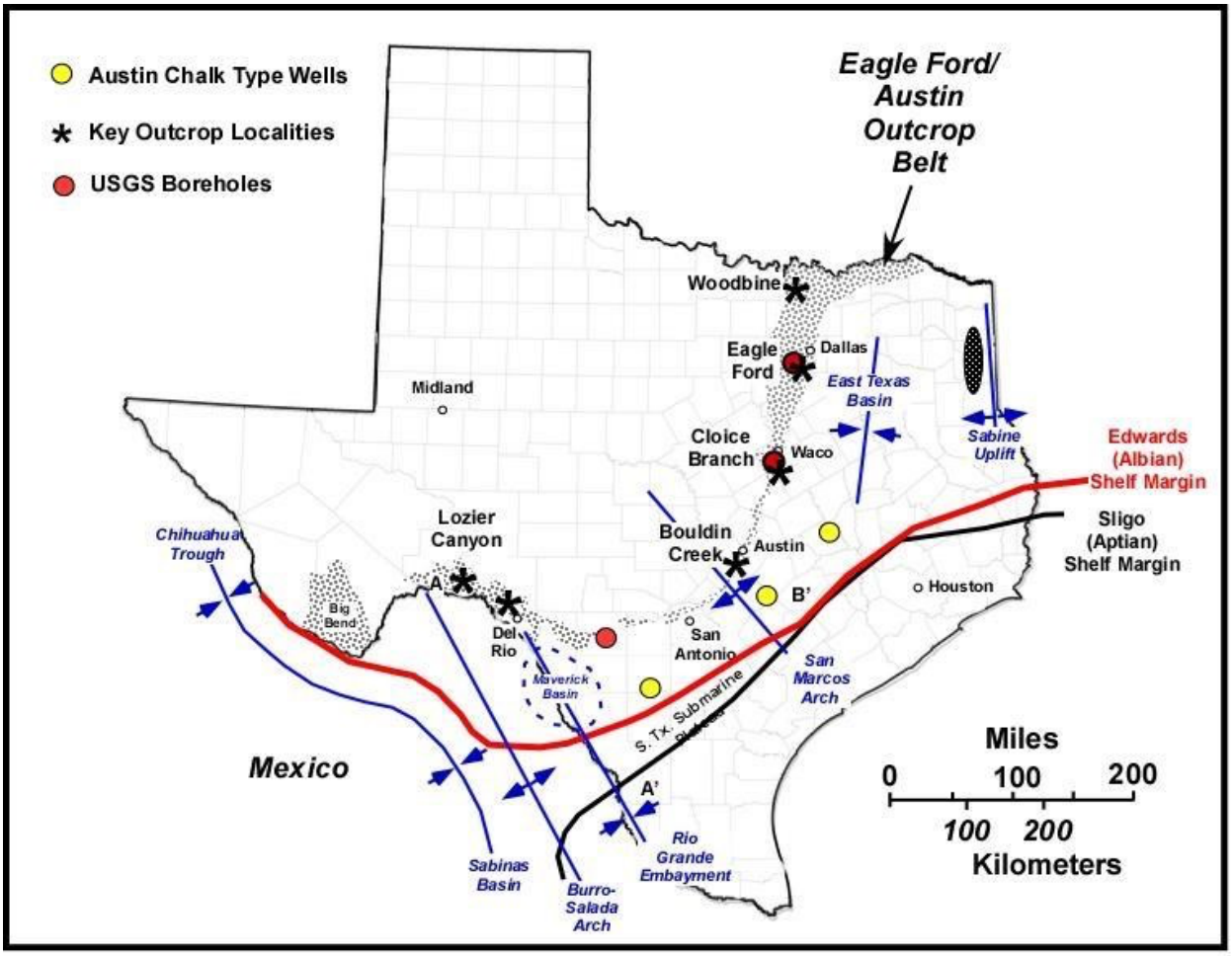

Figure 1. Basemap of Upper Cretaceuous rocks in the study area. The six wells used in this study are indicated by red circles (USGS boreholes GCA 1, 2, 3) and oil and gas wells by yellow circles (Getty Lloyd Hurt 1, Sallie Clark, and Well "X"). The position of the Sligo and Edwards shelf margins are modified from Donovan et al., 2019. Uplifts and basins across the study area are shown by the blue lines with arrow points.

Austin Group Geologic Setting

Beginning in the Middle Cenomanian and extending into the Campanian (Figure 2), global

seas rose and flooded the Early Cretaceous continental shelf, and epicontinental seaways, located at the southern end of the Western Interior Seaway (Huber et al., 2002, Vail et al., 1977). Over time, global greenhouse climate conditions accompanied the drowning of the platform and led to an increase in carbonate deposition as marked by the Austin Group. According to Hovorka and Nance (1994), the Austin Group was deposited in a shallow marine environment in water depths ranging from 30 to 300 feet (9 to 91 meters). The San Marcos Arch (Figure 1) separated Austin deposition in south and west Texas, from the East Texas Basin to the northwest (Adkins, 1933). The deposition of the Austin Group, across the state of Texas, also demonstrates both gradual lateral facies changes, as well as interpreted high-frequency sequences (Cooper et al., 2020).

The Austin Group is classically interpreted as a succession of fossiliferous wackestones (chalks), interbedded with (clay-rich) marl layers. It was deposited parallel to the ancient Gulf of Mexico continental shelf during an interpreted 2nd-order transgressive-regressive cycle (Hovorka and Nance, 1994, Cooper et al., 2020), that spanned the Latest Turonian through Middle Campanian (Figure 3). The Austin Group is an unconformity bounded unit, which overlies the Middle Cenomanian to Late Turonian Eagle Ford Group, and is overlain by the Campanian Taylor Group (Figure 3). The abundance and diversity of trace fossils (Planolites, Thallassinoides, and Chondrites) indicate that Austin Group deposition occurred in a well-oxygenated open marine environment (Dawson and Reaser, 1990).

Thickness of the Austin Chalk ranges from 145 to 787 feet (45 to 240 meters), depending on geographic location (Pearson, 2012). In south Texas (Figure 1), the strata are over 600’ (200 m) thick, but thin to less than x’ (y m) thick across the San Marcos Arch in central Texas. Outcropping northeast to southwest, the Austin Chalk outcrop belt extends from Oklahoma in the

North Texas to the Big Bend National Park region in the West Texas (Figure 1). The Austin Group is commonly divided into three units: the lower chalk, the middle marl, and the upper chalk (Hovorka and Nance, 1994). This subdivision is odd, in that the basal and upper boundaries are based on unconformities, but the internal lower/middle and middle/upper boundaries are picked at regional flooding surfaces.

Within the framework of Hovorka and Nance (1994), the lower Austin Chalk consists of alternating chalk and marl. The middle Austin has a higher authigenic clay content, that could be due to the mixing of volcanic ash or increased siliciclastic sediment input. The upper Austin Chalk has fewer marl laminations and thicker successions of chalk.

Figure 2: Paleogeographic map of the Late Cretaceous Western Interior Seaway during the Santonion of the Late Cretaceous with a red box indicating the study area (Modified from Blakey, 2019).

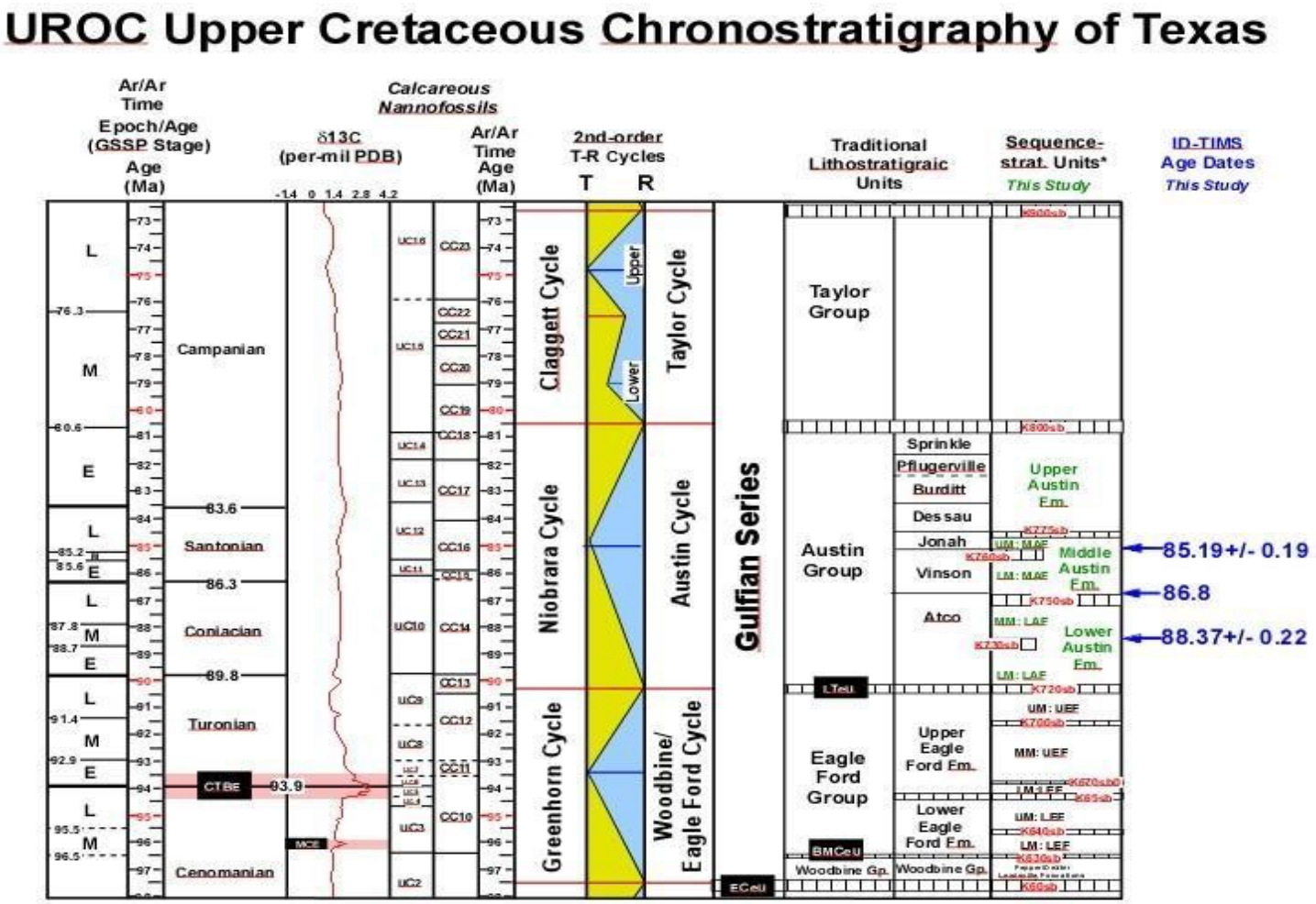

Figure 3: Upper Cretaceous Chronostratigraphic chart of Texas, constricted using Ar/Ar isotopes, $\delta^{13}C$ isotope profile, 2nd-order transgressive and regressive cycles, lithology, and traditional sequence-stratigraphic units.

METHODS

Study Area

The study area of the Austin Group extends across South and West Texas (Figure 1). The USGS partnered with Texas A&M University's Unconventional Reservoir and Outcrop Characterization (UROC) Consortium to perform a geochemical suite of analyses on three cores: the GCA1, near Waco, the GCA2 near Dallas, and the GCA3 near Uvalde. One industry core, the Getty 1 Lloyd Hurt, located in La Salle County, contains a nearly complete section of the Austin Group and was studied for key chemostratigraphic and elemental signatures to develop a regional sequence stratigraphic framework for the Austin Group. In addition to these four cores, the Sallie Clark well in Caldwell County, Texas was scanned, to provide insights into the Austin Group in the southern (deeper) portions of the East Texas Basin. These five cores were non-invasively sampled using a Bruker 5i hand-held X-Ray Fluorescence (XRF) unit. This elemental data was then depth plotted with the corresponding geophysical logs (e.g., gamma ray, resistivity, density-neutron) using Schlumberger's Techlog program to combine the elemental and petrophysical signatures of the defined chronostratigraphic units.

XRF Sampling and Data Acquisition

Energy dispersive, high-resolution XRF elemental data were collected using a Bruker Tracer 5i handheld spectrometer on the GCA 1, GCA 2, GCA 3, the Getty 1 Lloyd Hurt (GLH), and the Sallie Clark wells. The Tracer 5i was calibrated using the Bruker Geoexploration and the Bruker

Dual Mudrock Air calibrations. The core samples were scanned every 10 cm on the GCA cores, every 12 cm on the Sallie Clark core, and every 15 cm on the GLH core. The GCA cores were scanned during August 2019. The GLH core was scanned in January 2020.

During XRF sampling, at the beginning of each morning and afternoon, the XRF unit was warmed up for 5 minutes by scanning a silver pellet and two mudrock pellets of known mineral composition. This allowed for calibration checks during the day and at the end of each day to ensure confidence in the calibration settings. Before each sample was scanned, warm water was used to gently wash the sample, wiping away the excess water in the direction of the bedding plane. Water was not permitted to be used on the GCA 2 core, due to the excessive amount of bentonite beds in the core. Instead, dirt was removed from this core by dusting off surficial dust. After cleaning, the XRF unit was positioned face down on the evenly slabbed core to properly place the 10 cm by 12 cm window flush against the sample to create a closed environment for the XRF. Each sample was sequentially scanned for both major and trace elements, both for 30 second counts.

The Bruker XRF units are capable of analyzing the major (Na, Mg, Al, Si, P, S, K, Ca, Ti, Mn, and Fe) and trace (V, Cr, Ba, Co, Ni, Cu, Zn, Ga, As, Rb, Sr, Y, Zr, Nb, Mo, Pb, Th, and U) elemental composition of a rock sample (Rowe et al., 2012). After each scan, the elemental data was stored on an Excel sheet that also includes depth, time, calibration settings, and scan times. Where the XRF could not detect an element or the concentration is negligible, the instrument printed “LOD”, which stands for “Below Level of Detection” and is considered a null, non-valid value. These Excel sheets were plotted (Figures 4 - 8) into Techlog™ to correlate with the corresponding geophysical logs associated with the wells. To better aid in analysis, when the samples were originally collected, the core was described in EasyCore™. Pairing the

Techlog™ and EasyCore™ data sets allowed us to assign each sample with a lithofacies designation. Elemental proxies determined using XRF analysis were then used to help understand mineralogical trends associated with facies changes within the Austin Group.

Sequence Stratigraphic Correlation and Cross Sections

Correlating the Austin Group on well-log cross sections across the study area proved difficult without first establishing a nomenclature method within the Austin Group. Sequence stratigraphic surfaces were correlated building on a naming scheme used by Donovan and others (2019) in the Eagle Ford Group. Key surface boundaries as seen on geophysical logs and within chemostratigraphic data were labeled "mfs" for maximum flooding surfaces or "sb" for sequence boundaries. Within the Upper Cretaceous, the nomenclature calls for defining these boundaries using the letter "K" for Cretaceous, followed by surface designation numbered from the base up. Within this framework, the base of the Austin Group was designated as "K720sb" and the top of the Austin Group was labeled as "K800sb. Internal surfaces within the Austin Group were thus assigned numbers between K720 and K800. This methodology proved useful for accurately correlating key surfaces on well-log cross sections both laterally and vertically over a structurally complex and geographically large study area.

Field Study Methods

The outcrop type locality for the Austin Chalk is best exposed along US Highway 90 in Terrell County, Texas, just west of the town of Langtry, Texas (29.831, -101.629). Correlations using bentonite layer ash dating and sequence stratigraphic interpretations previously tied the outcrop to the subsurface using geophysical logs and field methods (Corbett et al., 2014; Freeman,

1961; Lowery, 2013; Minisini et al., 2018). A Bruker 5i XRF unit commonly is not taken into the field to collect samples for a myriad of reasons. The first being that the x-ray detector window of the XRF unit is only protected by a millimeter- thin layer of plastic. If this layer is damaged or torn, the film must be immediately replaced to prevent dust from damaging the detector and the XRF unit must be recalibrated within a laboratory setting. Additionally, when using the Mudrock Dual air calibration, the unit must be held against the sample for a minimum of thirty seconds to pass the level of detection for elemental collection.

These challenges were known prior to the field experiment in this study and were used to help plan for data collection. The outcrop has significant exposure to wind and water erosion and a metal grill brush was used to clear away dirt and biological residue growing on the surface. Next, to obtain a flat, uneroded surface on the outcrop, a Dremel 2050-15 tool with a diamond bit was used to smooth the surface intended for scanning. The dust was then cleared from the smoothed area, creating a 10 millimeter by 10 millimeter flat surface. One hundred measurements were collected, starting five feet below the Eagle Ford-Austin Group boundary, extending to ninety five feet above the boundary. A scan was measured every foot (30 centimeters). The outcrop was previously measured (see Griffith et al., 2019) and scanning intervals were indicated by adjacent strips of duct tape (Figure 4, B). The tape was used for depth referencing the scanning while walking along the outcrop. Pieces of tape were removed after sampling.

With no previous studies or indications on the viability of the XRF outcrop measurements, the field team also sampled core plugs every foot of the 95 feet (29 meters) of outcrop and transported the core plug samples to the laboratory to be scanned. A Tanaka TED-270 PFDH dualhandle, gasoline-powered core drill was used to drill 5 cm (1.5 inch) diameter core plugs from

the Langtry outcrop. These plugs took two full days to collect, then were cleaned, slabbed, and scanned (Figure 5).

Figure 4: A (label as A and B): Austin Chalk outcrop, located along Highway 90 4.5 miles (7.2 kilometers) west of Langtry, TX showing alternating marls and highly fractured massive sections of chalk. B: Scott Gifford gathering data with the Bruker 5i XRF unit against a cleaned, buffed, flat section of the outcrop. The silver duct tape marks the approximate locations of samples every 30 cm.

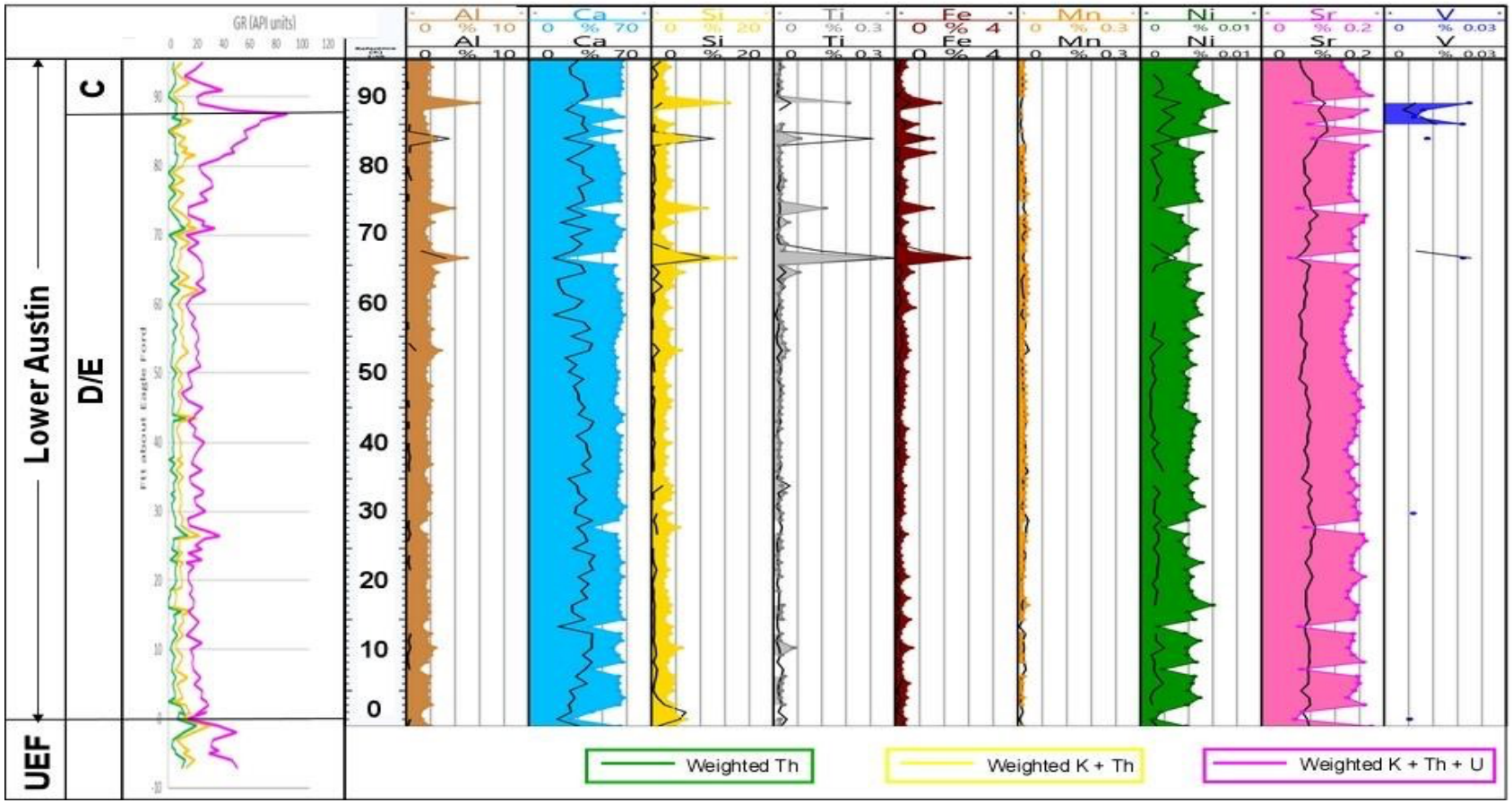

Figure 5: Plot of spectral gamma ray adjacent to an XRF plot of the Austin Group outcrop along Hwy 90 near Langtry, TX. On the spectral gamma ray, Th is green, K + Th is yellow, and K + Th + U is pink. On the XRF plots, the black lines indicate the XRF values collected on the surface of the outcrop; the color filled overlay are the XRF data collected from the powdered core samples.

RESULTS

Outcrop XRF Results

Dissimilarities between the Austin Group scanned direct outcrop and scanned cored outcrop samples are starkly apparent (Figure 5). Black lines indicate the XRF outcrop values overlain on the color filled points of the cored samples. Aluminum outcrop (Alo) appears to barely register on the curve, not even equating to 25% of the aluminum core (Alc) values. Calcium and strontium outcrop concentrations both show approximately 50% of the scanned core counterparts. The 97 feet (29.6 meters) outcrop is primarily composed of massive beds of calcium carbonate alternating with thinner marl beds; thus it is expected that the only two consistent, continuous outcrop curves are those of Cao and Sro. However, the trend of the outcrop results shows a significant decrease in concentrations when compared to the cored results throughout the entire elemental suite. Sio, Tio, and Feo outcrop values are almost nonexistent except when there are spikes in the cored sample values. At these depths, the elevated values of the outcrop equate those of the cores. Bioturbated marlstone beds occur from 85 to 89 feet (25 to 27 meters). Sedimentary structures within this interval include hummocky cross stratification and thin laminations.

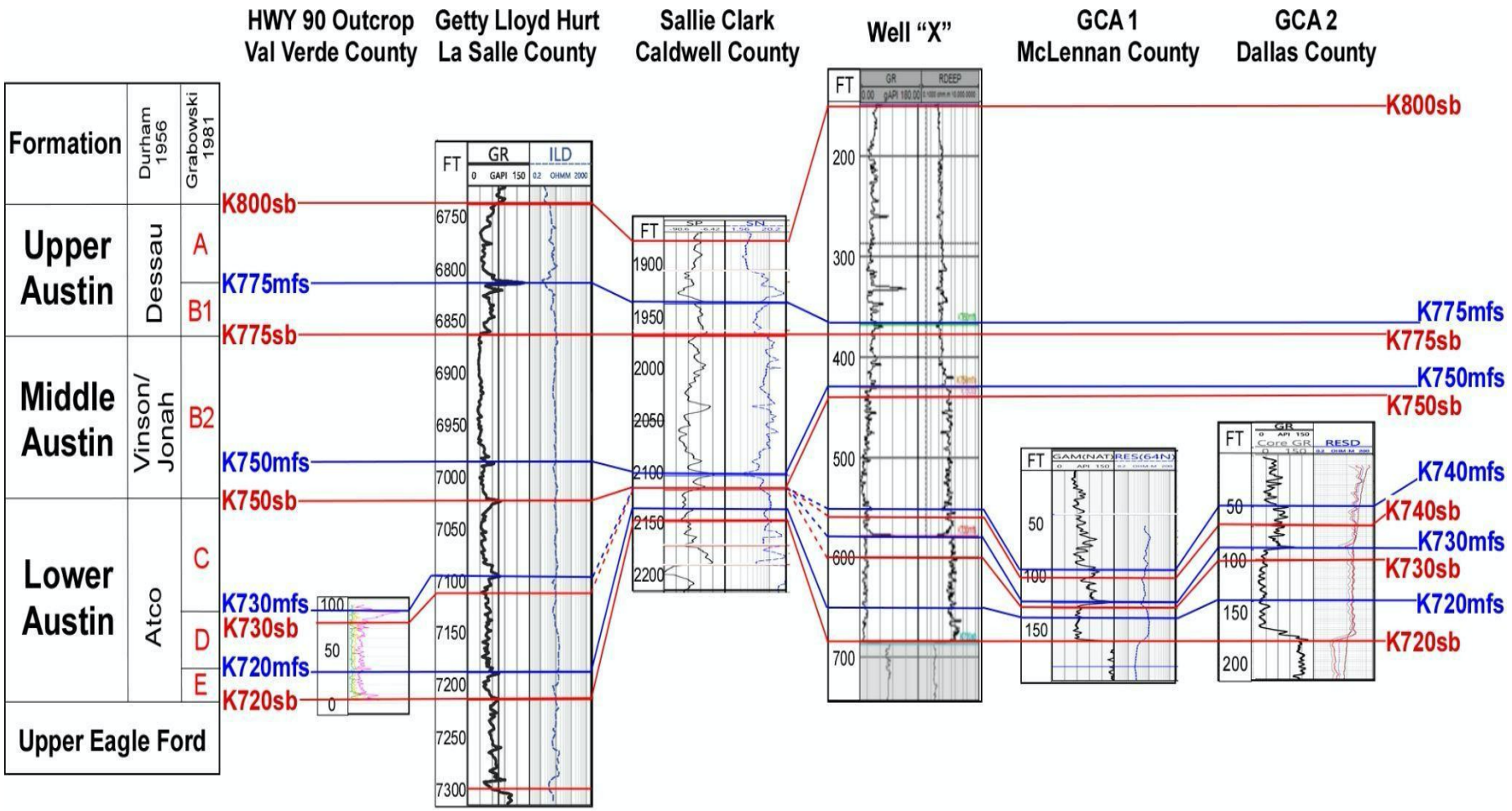

Figure 6: Correlation diagram of Austin Group wireline logs used in the study area highlighting key stratigraphic sequence boundaries in red (sb) and maximum flooding surfaces in blue (mfs). Each well shows gamma ray and resistivity curves. Crosssection hung on K775 sb between Middle and Upper Austin Formations. Lateral and vertical changes in Lower Austin thickest off and away from the San Marcos Arch in wells Getty Lloyd Hurt and Well "X".

Sequence Stratigraphy

Figure 6 is a SW-NE cross section that illustrates the large thickness variations of the Austin Group from Val Verde County in West Texas to Dallas County in North Texas. Of the five wells, as well as the type locality outcrop section, the Lower Austin Formation occurs in each section. What is designated as the Lower Austin Formation section in this cross-section previously was interpreted as the Atco Formation (Durham, 1956) and a combination of the C, D, and E units (Grabowski, 1981). This interval is characterized by a "boxcar" base with low gamma ray values from the K720 sequence boundary to the K730 maximum flooding surface, then a decrease in the gamma ray values until the K750 sequence boundary. The Lower Austin Formation is about two hundred feet thick in the Getty Lloyd Hurt well in LaSalle County and thins to the north to less than fifty feet in the Sallie Clark well in Caldwell County. Well "X" is located in the ETB, over one hundred miles east and downdip of the Sallie Clark well in Brazos County. The ETB log shows an increased thickness of the Lower Austin Formation, whereas the GCA 1 well is located alongside the Cretaceous outcrop belt.

The Middle Austin Formation is bounded at the bottom by the K750 sequence boundary and capped by the K775 sequence boundary at the top. It consists of the Vinson and Jonah Formations in outcrop as well as unit B2 in the subsurface (Grabowski, 1981). In this study, the Middle Austin Formation only occurs in three wells: the Getty Lloyd Hurt, the Sallie Clark, and Well "X". Elsewhere this unit was cut out by an unconformity or is currently weathered out. The Upper Austin Formation of this study consists of the Dessau Formation from outcrops and the A and B1 units in the subsurface, containing the highest values of the gamma ray of the three parts of the Austin Group. The Upper Austin Formation occurs in the Getty Lloyd Hurt, the Sallie Clark,

and Well “X”. This is consistent with the geographical location of the three wells being significantly more downdip of the outcrop belt than the other wells in this study.

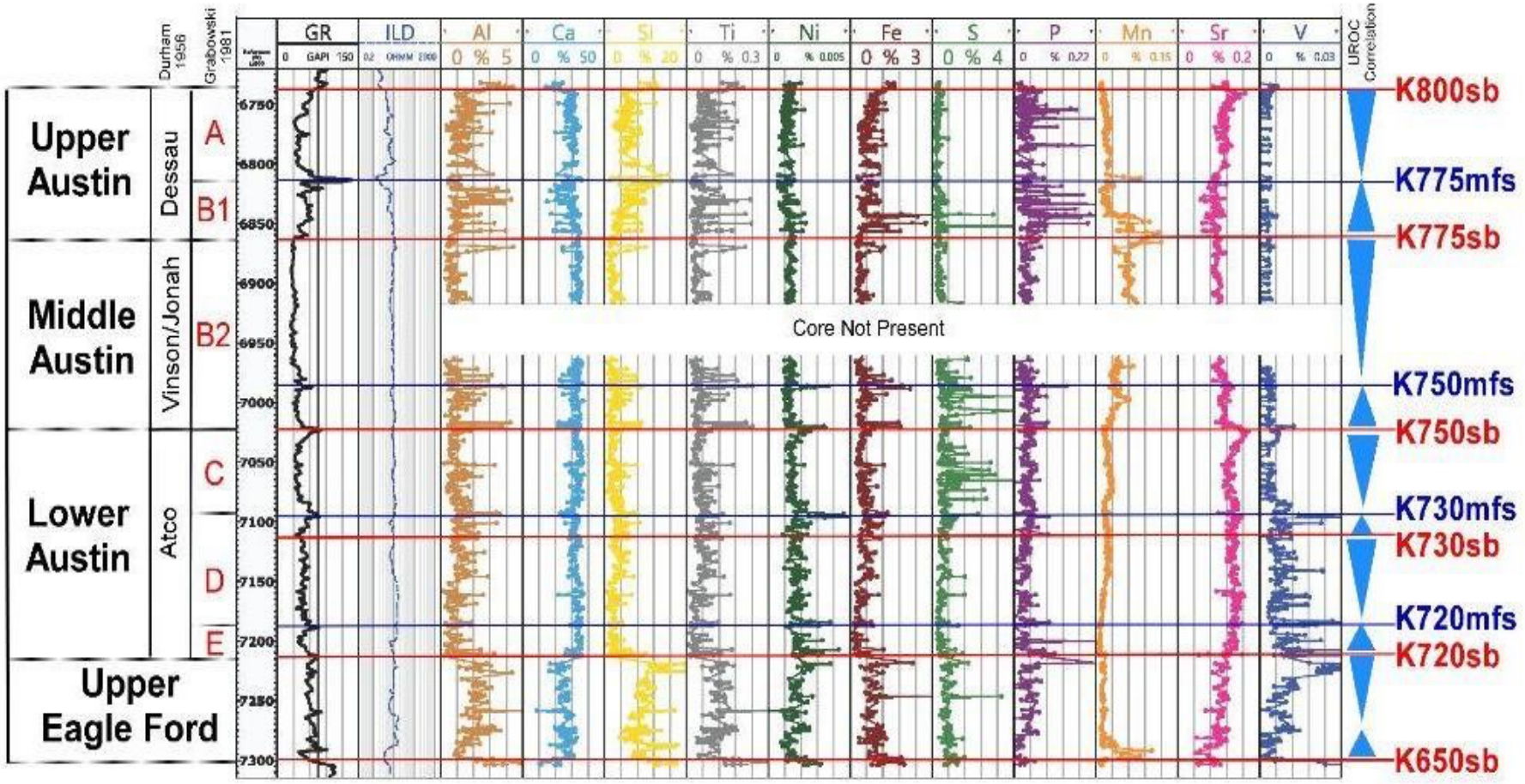

Figure 7: XRF elemental suite of the cored Getty Lloyd Hurt 1, collected by the Bruker Tracer 5i. Interpreted sequence boundaries and maximum flooding surfaces marked with red and blue lines respectively. Upper Eagle Ford, Lower Austin, and Upper Austin Formations marked. TSTs and HSTs within sequences indicated as blue triangles. TST triangles come to a point upward whereas HST triangles broaden upward.

Of the wells drilled in the Austin Group, the Getty Lloyd Hurt is the most extensively studied because it contains what is considered the full section of the laminated, marly chalk (Loucks et al., 2020). The geochemical facies in this well were well documented and published by previous researchers (Loucks et al., 2020). This study aims to correlate this well to others throughout the state using XRF chemostratigraphy confined by sequence stratigraphic markers. Chemostratigraphy used in conjunction with the sequence boundaries and maximum flooding surfaces better characterize the distinctive depositional profiles of the Austin Group at a much higher resolution than correlating solely with geophysical logs.

As mentioned previously, in this study, the Austin Group (Figure 7) is sub-divided into a Lower Austin Formation (LAF), a Middle Austin Formation (MAF), and an Upper Austin Formation (UAF). The LAF shows increased elemental concentrations of calcium, vanadium, and strontium. Between the K750sb and the K775sb, the MAF shows a slight decrease in calcium levels, significantly lower levels of vanadium and strontium, and a notable increase in aluminum, silica, titanium, and manganese. About seventy feet of the Getty Hurt was unaccounted for in the boxes, and therefore could not be scanned with the Bruker XRF unit. The UAF does not occur in North Texas but is over 100 feet (20 meters) thick in South Texas (LaSalle County) and over 200 feet (60 meters) thick in the East Texas Basin.

DISCUSSION

Hand-Held XRF Unit Use on Outcrop

The Bruker 5i XRF hand-held unit was used in the field for two reasons: 1) evaluate the viability of even using a hand-held XRF unit on an outcrop when it is traditionally only used on slabbed cores; and 2) compare the outcrop values with the core sample values under the same air calibration. While the results of the outcrop scans averaged around 25-50% of the cored samples values, future research should test these values with a helium calibration. A helium filled chamber during scans would ensure higher elemental counts which could elucidate if the outcrop versus core value discrepancies is due to calibration error or possibly due to movement of the unit while holding it against the outcrop.

Although there are lower overall values in the outcrop curves, the elemental trends still follow that of the cored data. Thus, while bringing a hand-held XRF unit into the field is a risky task with such an expensive instrument and large room for error, it is a useful tool for characterizing chemostratigraphic trends of an outcrop if samples cannot be gathered. This method would be applicable in National Parks or other remote areas where the goal of research and data collection is non-invasive.

Chemostratigraphy

Trace element concentrations in XRF chemostratigraphy are used as proxies (Table 1). For example, calcium (Ca), silicon (Si), and aluminum (Al) were used as proxies for carbonate, quartz, and clay input respectively in this study. Al, Si, and Ti were interpreted to indicate detrital input in depositional processes (Calvert and Pedersen, 1993). Iron (Fe), molybdenum (Mo), manganese

(Mn), and vanadium (V) were used to determine paleoceanographic oxic and redox conditions (Algeo and Rowe, 2012), whereas potential source rock organic matter preservation can be determined by molybdenum and vanadium (Tribovillard et al., 2006). Chemostratigraphic variations in the Austin Group are discerned by using elements calcium, strontium (Sr), and manganese that record carbonates that undergo wet subaerial-shallow subtidal diagenetic processes (Magaritz, 1974; Renard, 1979).

XRF elemental suite provides insight into small geochemical changes that are not always determined from the gamma ray and resistivity curves alone. For example, decreases in Al, Si, Ti, and Fe at the base of the Austin Group are more significant than any values within the Austin Group itself, indicating that the switch from Upper Eagle Ford Group to the Lower Austin Formation marks a (unconformable) boundary across which sharp differences in the oceanic geochemical conditions existed (Figure 7).

Within the Lower, Middle, and Upper Austin Formations, Al, Si, Ti, and Fe cyclically increase and decrease between the sequence boundaries and maximum flooding surfaces. Values in the Middle and Upper Austin Formations increase before the maximum flooding surfaces and decrease prior to the sequence boundaries, mirroring the gamma ray curve variations. S values between the depths of 6950 feet and 7110 feet show two large increases in concentrations that are not seen in the lower portion of the Lower Austin Formation or in the Upper Austin Formation (Figure 7). Within the Upper Austin Formation, P shows two dramatic pulses of values, but otherwise shows low values in the Middle and Lower Austin Formations. From the bottom of the core to the Middle to Upper Austin Formation boundary, Mn values gradually rise before peaking at the K775 sb at 6860 feet. Mn and P values increase below sequence boundaries where glauconite occurs in the core above the Middle-Upper boundary. Glauconite is formed in shallow marine

environments that are mildly reducing, thus a period of reducing conditions most likely occurred between K775 sb and K775 mfs when the Mn is decreasing, Fe is increasing, and other clay inputs began to increase dramatically.

	Mineralogy	Proxy	Interpretation	References
Al	Clay minerals. Illite Group. Glauconite.	Clay and Feldspar	Concentration of clay and feldspars in limestones can be used to help identify sections of clay input and interbedded marls.	Pearce & Jarvis (1992); Tribovillard *et al.* (2006)
Ca	Calcite ($CaCO_3$), Calcium orthophosphates ($CaPO_4$)	Carbonate source and Phosphate accumulation	Calcium is primarily a proxy for calcite and calcareous input in limestones.	Banner (1995); Tribovillard *et al.* (2006)
Si	Quartz (SiO_2)	Quartz	Silica is used as a proxy for quartz and terrigenous input.	Pearce & Jarvis (1992); Sageman & Lyons (2004)
Ti	Detrital sediments (Ti^{4+}, Rutile (TiO_2), and Ti-bearing minerals)	Continental source and dust fraction; Intensity of chemical weathering	Titanium and other detrital elements are used as proxies to interpret depositional processes, like source origin and weathering, versus paleooceanographic conditions	Calvert & Pedersen (1993); Sageman & Lyons (2004)
Ni	$NiCO_3$, Ni^{2+}, $NiCl^{+}$ (oxic conditions); NiS (sulfate reducing conditions)	Organic matter/micronutrient availability in the water column	Ni is soluble in oxygenated water columns and behaves as a micronutrient for microbial scavengers. In stratified water columns or upwelling, scavengers will ingest Ni in oxygenated surface waters and will be deposited and preserved at the anoxic sediment-water interface.	Tribovillard *et al.* (2006)
Fe	Pyrite (FeS2), Ferroan Dolomite ($Ca(Mg, Fe)(CO_3)_2$), Siderite ($FeCO_3$)	Redox sensitive	Trace metals that are redox sensitive are useful for characterizing oxic/suboxic/anoxic paleooceanographic conditions during time of deposition.	Tribovillard *et al.* (2006)
S	Pyrite (FeS_2)	Redox sensitive	Trace metals that are redox sensitive are useful for characterizing oxic/suboxic/anoxic paleooceanographic conditions during time of deposition.	Tribovillard *et al.* (2006)
P	Phosphates Apatite($Ca_5(PO_4)_3(Cl/F/OH)$)	Phosphate accumulation; Upwelling	PO_4^{3-} is released from decaying organic matter. However, it can either escape back to the water column or be trapped within the depositing sediment. Thus, it is not an independently reliable productivity/upwelling or redox proxy.	(Tribovillard *et al.* (2006)
Mn	MnO_2, Mn^{2+}/Mn(IV), and Mn(II) oxides	Redox sensitive, Mn-enrichment during oxic bottom water conditions.	The mobile nature of Manganese in reducing conditions allows for ease of transfer of trace metals out of the water column and into the depositing sediment. Upwelling sediments are low in Mn-enrichment.	Calvert & Pedersen (1993); Sageman & Lyons (2004); Brumsack (2006)
Sr	Sr-Ca substitutes in calcite, aragonite and dolomite	Carbonate source and phosphate. Affinity towards calcium carbonate	With an affinity for substitution in carbonate forming minerals, Strontium is used as a proxy for carbonate source and diagenetic influence.	Scholle (1977); Renard (1979); Banner (1995);
V	HVO2-4 and H2VO-4 (oxic) VO2-, VO(OH)-3, VO(OH)2 (mildly reducing)	Bottom water anoxia, redox sensitive. Authigenic organometallic input	Redox sensitive trace metals help determine paleoceanographic conditions during deposition. Enrichment of Vanadium occurs in suboxic-anoxic conditions because it is immobile in low oxygen, restricted environments.	Sageman & Lyons (2004); Algeo and Rowe, 2012
Ba	Barite ($BaSO_4$)	Paleoproductivity	Barium is found as Barite in the water column and is associated with carbon export flux. In anoxic, sulfate reducing environments, barite is not preserved. Barium can reprecipitate as barite in oxic sediment layers, thus diagenetic alteration must be assessed to use Barium as a reliable proxy.	Griffith & Paytan (2012); Liguori *et al.* (2016)

Table 1. Geochemical proxies used for chemostratigraphic interpretation and mineralogy of collected datasets using handheld x-ray fluorescence (XRF) devices.

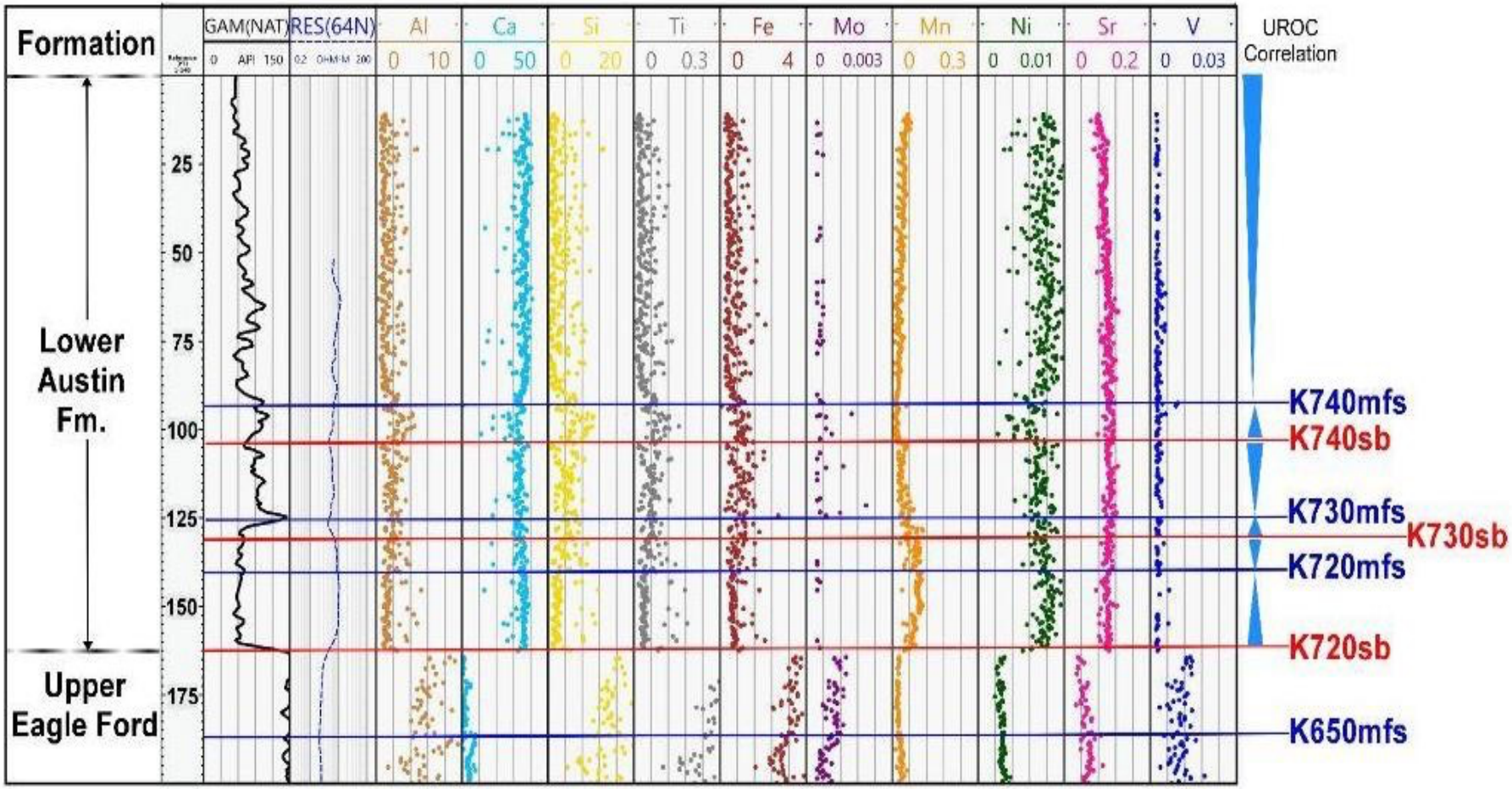

Figure 8: XRF elemental suite of the USGS GCA 1 core, collected by the Bruker Tracer 5i. Interpreted sequence boundaries and maximum flooding surfaces marked with red and blue lines respectively. Upper Eagle Ford and Lower Austin Formation marked. Sequences bounded by sequence boundaries contain upward pointing blue triangles (TST) and upward broadening blue triangles (HST).

At the base of the Austin Group, where the K720sb is placed, terrigenous and authigenic proxies decrease drastically, while calcium-carbonate proxies increase in value. This coincides with the sharp drop in gamma ray values at the base of the Austin Group. Throughout the Austin Group, V values are consistently low in comparison to the Eagle Ford Group values. This suggests that the Austin Group was deposited in oceans with higher O_2 concentrations, since V-enrichment occurs in suboxic- anoxic conditions as it is immobile in such low-oxygen environments (Helz et al., 1996, Sageman and Lyons, 2004, Algeo and Rowe, 2012). Ni is highest in the Lower Austin Formation in the GCA 1 well between the K720 sb and K730 mfs, as well as between K740 mfs and the top of the core. Ni is soluble in oxygenated marine settings and behaves as a micronutrient for microbial scavengers (Tribovillard et al., 2006). Between K730 and K740 mfs, Ni is the lowest of the Lower Austin Formation, whereas Mo and Fe, redox-sensitive proxies, are the highest, suggesting a period of reducing conditions before switching back to high levels of oxygenation in the water column.

The elemental suite of the GCA 1 well (Figure 8), located in McLennan County, shows a moderate influx of terrigenous inputs Al and Si from the K720 sb to the K740 mfs. In this well, the K740 mfs denotes a considerable boundary within the Lower Austin Formation separating this unit into a more carbonate-rich section from -90 feet to the surface. In this well, the Mo values are higher between the K730 mfs and the K740 mfs, suggesting a more anoxic section that does not occur in the sections below and above these bounding surfaces.

The GCA 2 (Fig. 9) well is the northernmost well in this study and contains only the Lower Austin Formation. This section is carbonate prone and clay-poor (Figure 9). The K730 mfs and K740 mfs occur in both the GCA 1 and GCA 2 wells and both sections contain higher concentrations of Mo between these boundaries. Both Lower Austin Formation sections also

show similar bell-curved shape values of Mn abundance from the K720 sb to the K730 mfs. Conversely, only the GCA 2 well shows elevated values of V between the K720 sb and extending beyond the K720mfs. When only viewed by itself, the Lower Austin Formation has intervals of terrigenous inputs in a predominantly carbonate-rich section. However, when compared to the Middle and Upper Austin, the Lower Austin Formation is the more carbonate-rich section, with relatively lower Ti, Al, Si values.

In both the GCA 1 and GCA 2 wells, Mn shows a bell-curved shape between K720 sb and K730 sb before decreasing back to consistently low levels through the rest of the core (Figure 8, 9). Mn is a redox sensitive geochemical proxy and is enriched in oxic bottom water conditions and allows for transfer of trace metals out of the water column to be deposited into the sediment (Brumsack, 2006). However, due to the ease of Mn movement and transfer, Mn is an unreliable proxy when used alone and should be used in conjunction with other redox sensitive elements to determine bottom water conditions. The high Mn values in GCA 1 and GCA 2 paired with low enrichment of V, Mo, and Fe indicates both GCA wells records a period of higher oxygenation between K720 mfs and K730 mfs.

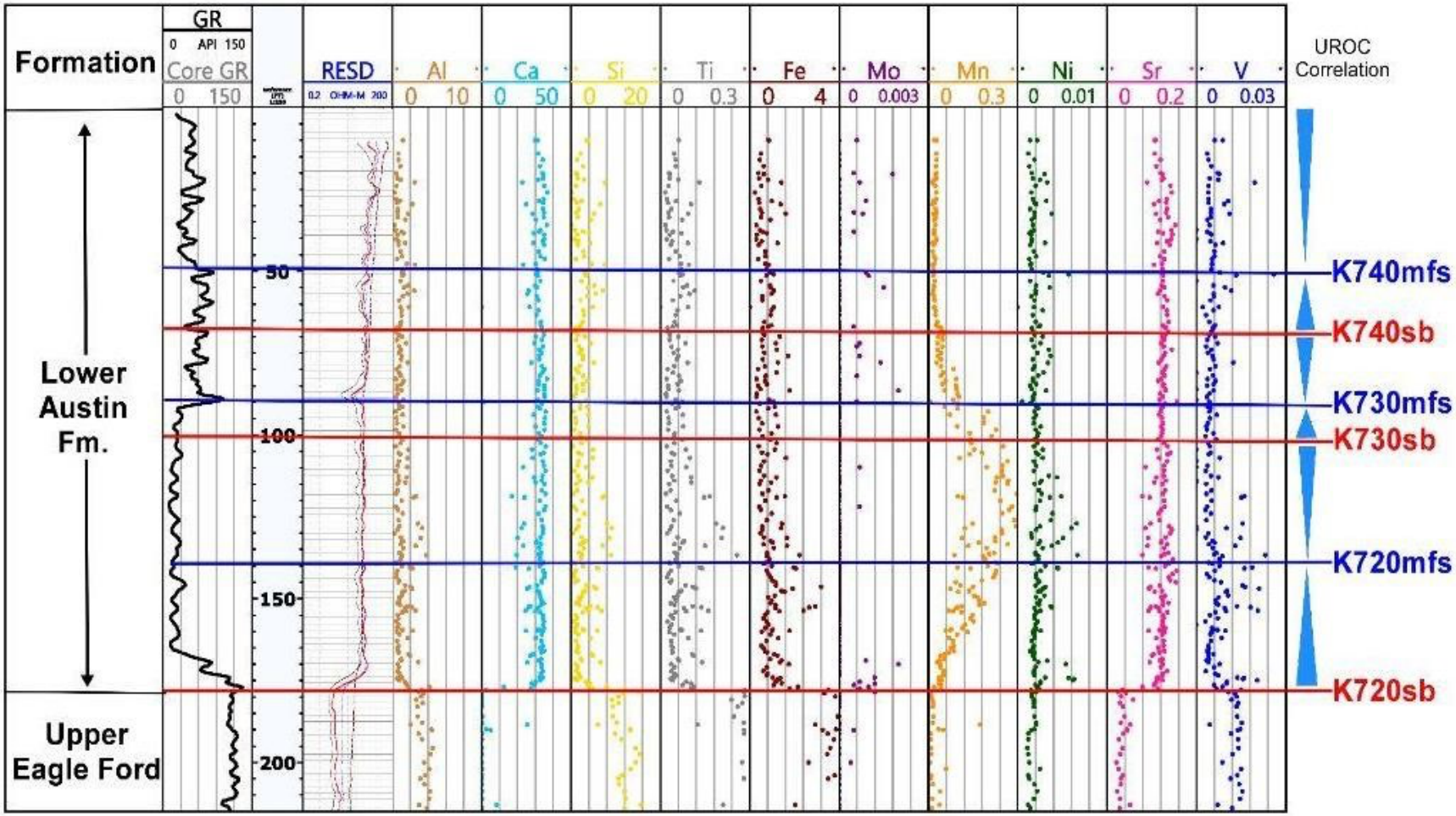

Figure 9: XRF elemental suite of the cored USGS GCA 2, collected by the Bruker Tracer 5i. Interpreted sequence boundaries and maximum flooding surfaces marked with red and blue lines respectively. Upper Eagle Ford and Lower Austin Formations marked. Sequences bounded by sequence boundaries contain upward pointing blue triangles (TST) and upward broadening blue triangles (HST).

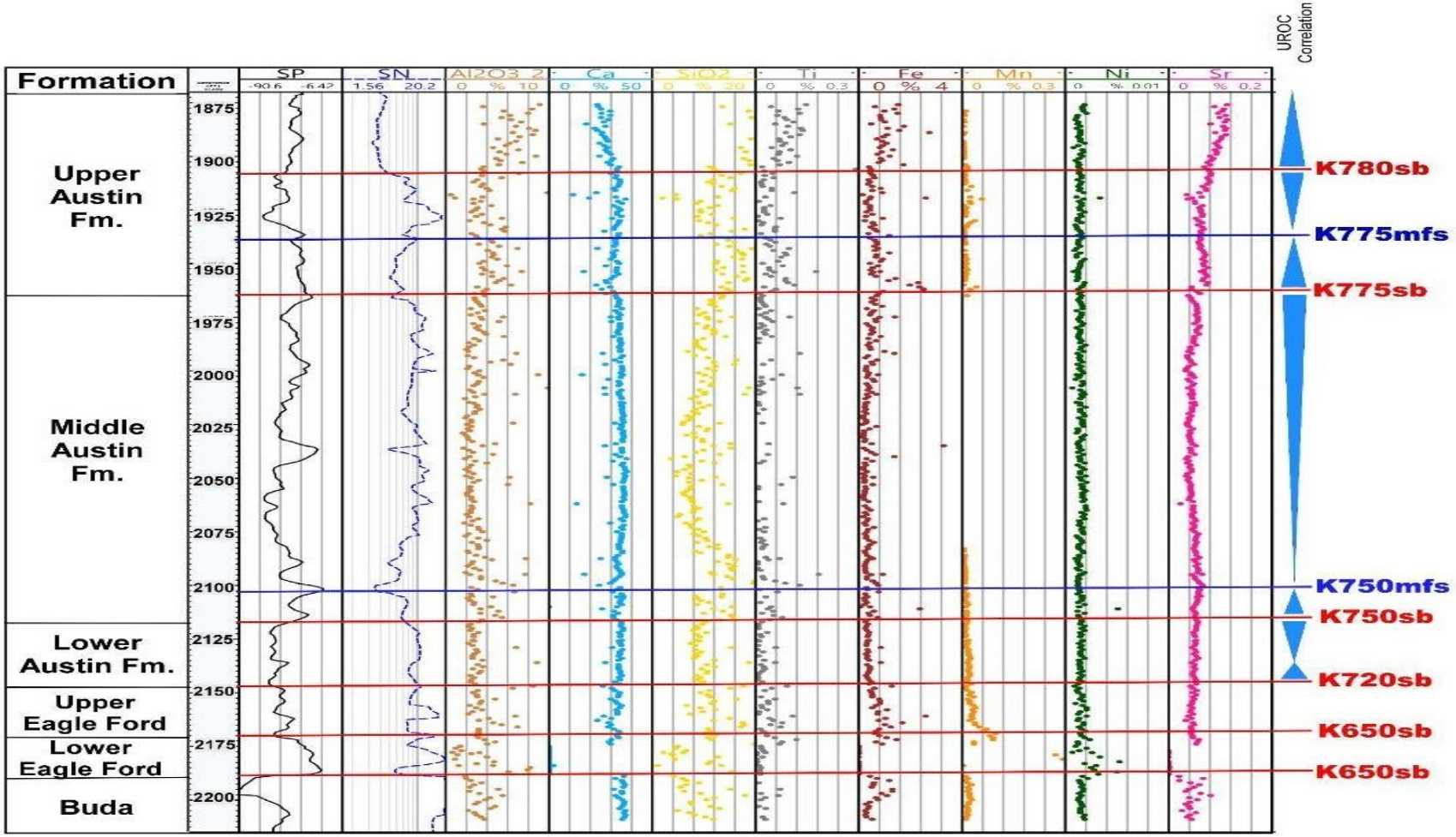

Figure 10: XRF elemental suite of the cored Sallie Clark well, collected with the Bruker Tracer 5i. Interpreted sequence boundaries and maximum flooding surfaces marked with red and blue lines respectively. Buda, Lower Eagle Ford, Upper Eagle Ford, Lower Austin, Middle Austin, and Upper Austin formations marked. S Sequences bounded by sequence boundaries contain upward pointing blue triangles (TST) and upward broadening blue triangles (HST).

The Sallie Clark well in Caldwell County, provides the best insights into the Austin Group as an entire geochemical entity, since its core spans the entire Austin (Figure 10). The Sallie Clark has a thin Lower Austin Formation (30 feet, 10 meters). The sequence boundary and maximum flooding surfaces were correlated between the Pearsall Field and the ETB, but the K740 sb and K740 mfs are missing from this section. This suggests that a significant portion of the Lower Austin Formation was eroded before the deposition of the Middle Austin Formation.

The base of the Middle Austin Formation is interpreted to be the beginning of argillaceous input and increased values of terrigenous inputs (Al,Ti,Si). Higher in the Middle Austin Formation, the Al values fluctuate, but not with as high intensity as the Si and Ti values. The Mn is nonexistent in the Middle Austin Formation, meaning the elemental counts were below level of detection. This could potentially be attributed to be an error upon collection or just low values within that section of the core. The top of the Middle Austin Formation and bottom of the Upper Austin Formation is demarcated by the K775 sb, with clear increase of argillaceous proxies above the boundary, coincident with a clear decrease of Ca values above the boundary.

CONCLUSIONS

XRF chemostratigraphic and petrophysical data, tied to detailed correlations of well log cross sections, provides a robust sequence stratigraphic framework to divide the Austin Group into three main unconformity bounded units termed the Lower, Middle, and Upper Austin Formations in this study. The Lower Formation is a carbonate prone, clay-poor chronostratigraphic unit that is the primary petroleum industry target in the subsurface. Our work reveals that it correlates to the US Hwy 90 outcrops in Val Verde County in West Texas, where this unit can be studied in detail.

At the base of the Austin Group, where the K720sb is place, terrigenous and authigenic proxies decrease drastically, while calcium-carbonate proxies increase in value. This coincides with the sharp drop in gamma ray values at the base of the Austin Group. Throughout the Austin Group, V values are consistently low in comparison to the Eagle Ford Group values. This suggests that the Austin Group was deposited in oceans with higher O2 concentrations, than the underlying Eagle Ford Group, which was deposited under more anoxic conditions.

The Lower Austin Formation becomes systematically more terrigenous (argillaceous-rich) northward towards Dallas. This facies change is interpreted to record a more proximal depositional environments within the Lower Austin Formation in this direction. Reducing conditions between K730 mfs to K740 mfs increased as seen by increases in Mo, Fe. Decreases in Mn and Ni in the same K730 mfs to K740 mfs section indicates decreasing paleo-productivity proxies. Mn is high in in GCA 1 and GCA 2 and throughout the entirety of the Lower Austin Formation in the Getty Hurt well, but not in the downdip Sallie Clark. Mn and P values increase below sequence boundaries where glauconite occurs above the Middle-Upper boundary.

Within the Middle Austin Formation, elemental values show initial argillaceous input and increased values of terrigenous inputs seen in Al, Si, and Ti values. The Middle Austin Formation

does not occur in the GCA wells closest to the Cretaceous outcrop belt. Within the Upper Austin Formation, a period of shallow water reduction most likely occurred between K775 sb and K775 mfs. Compared to the Lower and Middle Austin Formations, the Upper Austin Formation only occurs in downdip wells, but is not considered the best target for the petroleum industry, as it contains the highest values of argillaceous proxies, even though it appears to have been formed during reducing conditions. The Upper Austin Formation shows a significant increase in Al, Si, and Ti values, whereas Ca is lowest in all three wells. The Upper Austin Formation only occurs in the downdip wells: Getty Lloyd Hurt, Sallie Clark and Well "X".

With regards to petroleum industry interest in the Austin Group, the Lower Austin Formation is the traditional target, as it contains the least amount of clay and will not swell during drilling. Exploration in the Middle and Upper Austin Formations could be possible with a smaller, local scale investigation of clay inputs within various plays.

REFERENCES

Adkins, W. S., 1932, The Mesozoic systems in Texas, *in* z. H. Sellards, W. S. Adkins, and F. B. Plummer, eds., The Geology of Texas: University of Texas Bulletin 3232, p. 239-518.

Balamurali M. and Melkumyan A. (2016) t-SNE Based Visualisation and Clustering of Geological Domain. In: Hirose A., Ozawa S., Doya K., Ikeda K., Lee M., Liu D. (eds) Neural Information Processing. ICONIP 2016. Lecture Notes in Computer Science, v. 9950.

Banner, J. L., 1995, Application of the trace-element and isotope geochemistry of strontium to studies of carbonate diagenesis. Sedimentology, v. 42, p. 805-824.

Blakey, R., 2019. Global Paleogeography. *Global Series: Cretaceous.*

Brumsack, H-J., 2006,The trace metal content of recent organic carbon-rich sediments: Implications for Cretaceous black shale formation, Palaeogeography, Palaeoclimatology, Palaeoecology, v. 232, i. 2–4, p. 334-361.

Calvert, S.E. and Pedersen, T.F., 1993. Geochemistry of Recent oxic and anoxic marine sediments: Implications for the geological record. In: R.J. Parkes, P. Westbroek and J.W. de Leeuw (Editors), Marine Sediments, Burial, Pore Water Chemistry, Microbiology and Diagenesis. Mar. Geol., v. 113, p. 67-88.

Cooper, J., Godet, A., and Pope, M., 2020, Tectonic and eustatic impact on depositional features in the Upper Cretaceous Austin Chalk Group of south-Central Texas, USA. Sedimentary Geology.

Corbett, K., Friedman, M., and Spang, J., 1987. Fracture development and mechanical stratigraphy of Austin Chalk, Texas. AAPG Bulletin, v. 71, p. 17-28.

Dawson, W.C., and Reaser, D.F., 1990, Trace fossils and paleoenvironments of Lower and Middle Austin Chalk (Upper Cretaceous), north-central Texas: Transactions—Gulf Coast Association of Geological Societies, v. 40, p. 161–173.

Dawson, W., Katz, B., and Robison, V., 1995, Austin Chalk (!) petroleum system Upper Cretaceous, southeastern Texas: a case study GCAGS Transactions, v. 45, p. 157-163.

Ewing, T. E., and Caren, C. S., 1982, Late Cretaceous volcanism in south and central Texas: stratigraphic, structural and seismic models. Gulf Coast Assoc: Geol. Soc. Trans, v. 32, p. 137145.

Ewing, T.E., 1991, Structural framework. In: The geology of North America (Ed A. Salvador), Geological Society of America: Boulder, CO, p. 31–52.

Friedman, M., and D. E. McKiernan, 1995, Extrapolation of fracture data from outcrops of the Austin Chalk in Texas to corresponding petroleum reservoirs at depth: Journal of Canadian Petroleum Technology, v. 34, p. 43–49.

Griffith, E., and A. Paytan, 2012, Barite in the Ocean – Occurrence, Geochemistry and Palaeoceanographic Applications, Sedimentology, v. 59, p. 1817-1835.

Helz, G., C. Miller, J. Charnock, J. Mosselmans, R. Pattrick, C. Garner, and D. Vaughan, 1996, Mechanism of molybdenum removal from the sea and its concentration in black shales: EXAFS evidence Geochem. Cosmochim. Acta, v. 60 p. 3631-3642.

Hovorka, S.D., and Nance, H.S., 1994, Dynamic depositional and early diagenetic processes in a deep-water shelf setting, Upper Cretaceous Austin Chalk, north Texas: Transactions—Gulf Coast Association of Geological Societies, v. 44, p. 269–276.

Huber, B.T., Norris, R.D., MacLeod, K.G., 2002. Deep-sea paleotemperature record of extreme warmth during the Cretaceous: Geology 30, p. 123-126.

Kilcoyne, D., 2018, Mapping Lower Austin Chalk Secondary Porosity Using Modern 3-D Seismic and Well Log Methods in Zavala County, Texas. University of Arkansas, Theses and Dissertations. 2835, p. 1-86.

Liguori, B., M. Almeida, and C. Rezende, 2016, Barium and Its Importance as an Indicator of Paleoproductivity: Anais Da Academia Brasileira De Ciências, Academia Brasileira De Ciências, v. 88, p. 2093-2103.

Pearce, T., and I. Jarvis, 1992, Applications of geochemical data to modelling sediment dispersal patterns in distal turbidites- Late Quaternary of the Madeira abyssal plain: Journal of Sedimentary Petrology, v. 62, p. 1112–1129.

Pearson, K., 2012, Geologic models and evaluation of undiscovered conventional and continuous oil and gas resources—Upper Cretaceous Austin Chalk, U.S. Gulf Coast: U.S. Geological Survey Scientific Investigations Report 2012–5159, p. 26.

Pomerol, B., 1976, Géochimie des craies du Cap d'Antifer (Haute-Normandie). Bull. Soc. Géol. France, Paris, sér. 7, p. 1051.

Renard, M., 1979, Aspect géochimique de la diagenèse des carbonates. Teneurs en strontium et en magnésium des carbonates: essai d'interprétation de l'inversion de la corrélation SrMg observée dans les carbonates du domaine pélagique par rapport à ceux du domaine néritique. Bull. B.R.G.M. Sect. IV, 2, p. 133-152.

Robin, E., Rabouille, C., Martinez, G., Lefevre, I., Reyss, J., van Beek, P., Jeandel, C., 2003, Direct barite determination using SEM/EDS-ACC system: implication for constraining barium carriers and barite preservation in marine sediments. Mar. Chem., v. 82 (3–4), p. 289-306.

Rowe, H. D., Hughes, N., and Robinson, K., 2012, The quantification and application of handheld energy-dispersive x-ray fluorescence (ED-XRF) in mudrock chemostratigraphy and geochemistry. Chemical Geology, v. 324-325, p. 122-131.

Sageman. B., and T. Lyons, 2004, Geochemistry of fine-grained sediments and sedimentary rocks. In: Mackenzie, F. (ed.) Sediments, Diagenesis, and Sedimentary Rock: Treatise on Geochemistry, 7. Elsevier, Amsterdam, p. 115–158.

Schlanger, S., and H. Jenkyns, 1976, Cretaceous oceanic anoxic events: causes and consequences: Geologie en mijnbouw, v. 55, no. 3-4, p. 179–184.

Scholle, P., 1977, Chalk Diagenesis and Its Relation to Petroleum Exploration- Oil from Chalks, a Modern Miracle: AAPG Bulletin, American Association of Petroleum Geologists v. 61, no. 7, p. 982–1009.

Tribovillard, N., Thomas, J., Lyons, T., and Armelle, R., 2006, Trace metals as paleo-redox and paleo-productivity proxies- An update: Chemical Geology v. 232, p. 12-32.

Turner, B., and Tréanton, J., and Slatt, R., 2016, The use of chemostratigraphy to refine ambiguous sequence stratigraphic correlations in marine mudrocks. An example from the Woodford Shale, Oklahoma, USA. Journal of the Geological Society. p. 173.

Vail, P.R., Mitchum, R.M., Jr., and Thompson, Sam III, 1977, Seismic stratigraphy and global changes of sea level, part 4: Global cycles of relative changes of sea level, in Payton, C.E., ed., Seismic stratigraphy—Applications to hydro-carbon exploration: Tulsa, Okla., American Association of Petroleum Geologists Memoir, v. 26, p. 83–97.

L.J.P. van der Maaten and G.E. Hinton, 2012. Visualizing High-Dimensional Data Using tSNE. Journal of Machine Learning Research. p. 2579-2605.

APPENDIX

T-SNE Dimensionality Reduction

T-Distributed Stochastic Neighbor Embedding (t-SNE) is a non-linear dimensionality reduction algorithm that is used to further examine datasets with many identifying features (van der Maaten and Hinton, 2008). T-SNE designates patterns in the data by identifying observed clusters based on similarity of data points with multiple features (Balamurali and Melkumyan, 2016). Highdimensional XRF spreadsheets that combine full geochemical suites of elements showed promise in this study when using this low-dimensional reduction technique. The t-SNE dimensionality reduction algorithm used was originally developed by Liam Lauckner using R Studio™, but was converted to be used in Jupyter Notebook™ (anaconda3). T-SNE was applied to the XRF gathered points as a data visualization method that can create a multi-scaled, low-dimension map to distinguish between local and global scale differences (van der Maaten and Hinton, 2008). Other dimensionality reduction algorithms were considered for sorting and cluster visualization (e.g. Laplacian Eigenmaps(non-linear), PCA (linear)), but the t-SNE method best preserved the integrity of both the local (nearby points to nearby points) and global (nearby points to nearby points and faraway points to faraway points) geometries of the points on the manifold within the limits of this study (Balamurali and Melkumyan, 2016)

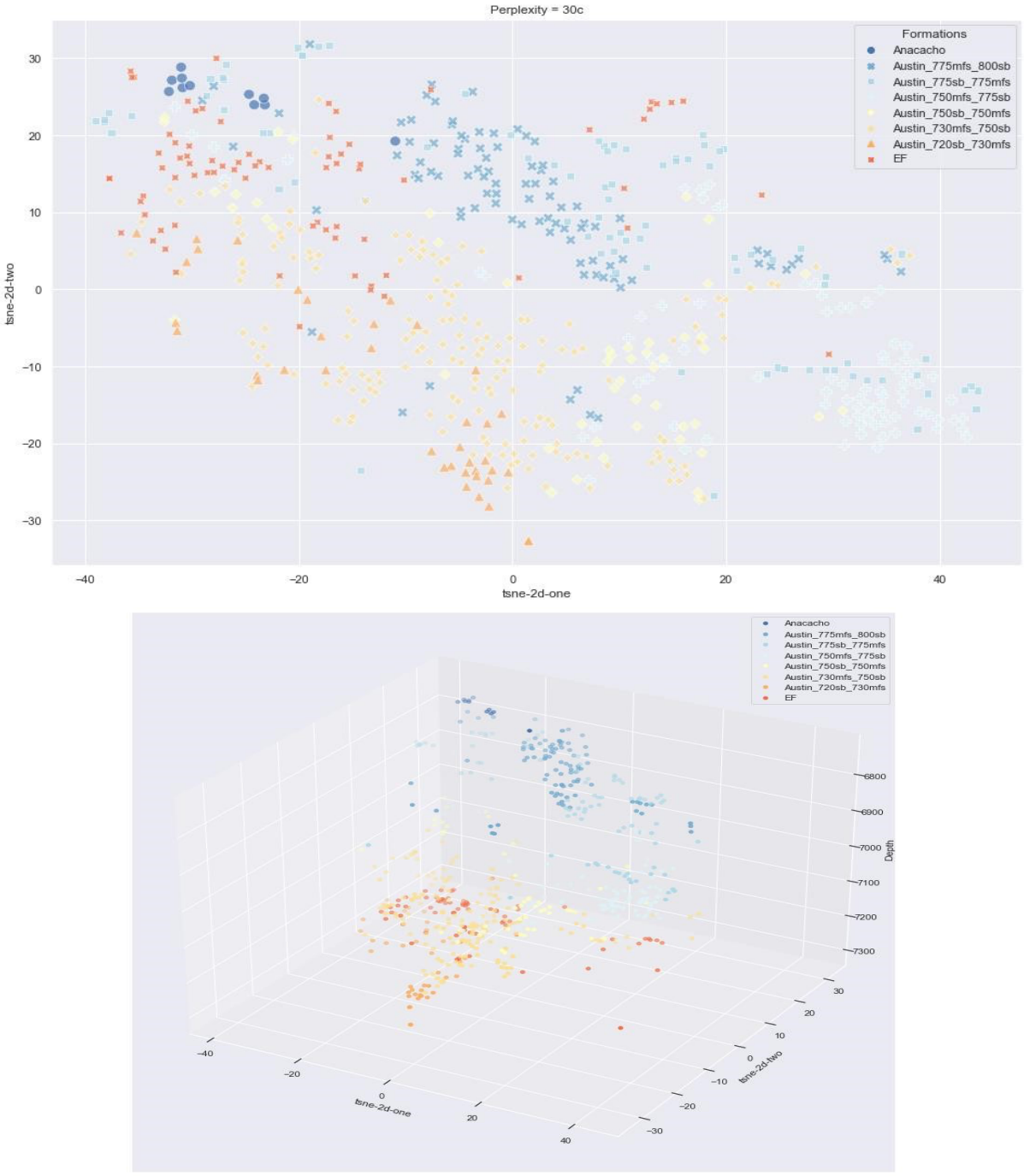

Figure 11: T-Distributed Stochastic Neighbor Embedding (t-SNE) of the Getty Lloyd Hurt well in 2D (top) and 3D (bottom). The perplexity is 30 on both plots. Points are distinguished by shape and color, delineated by key sequence boundaries and maximum flooding surfaces within the Austin Chalk.

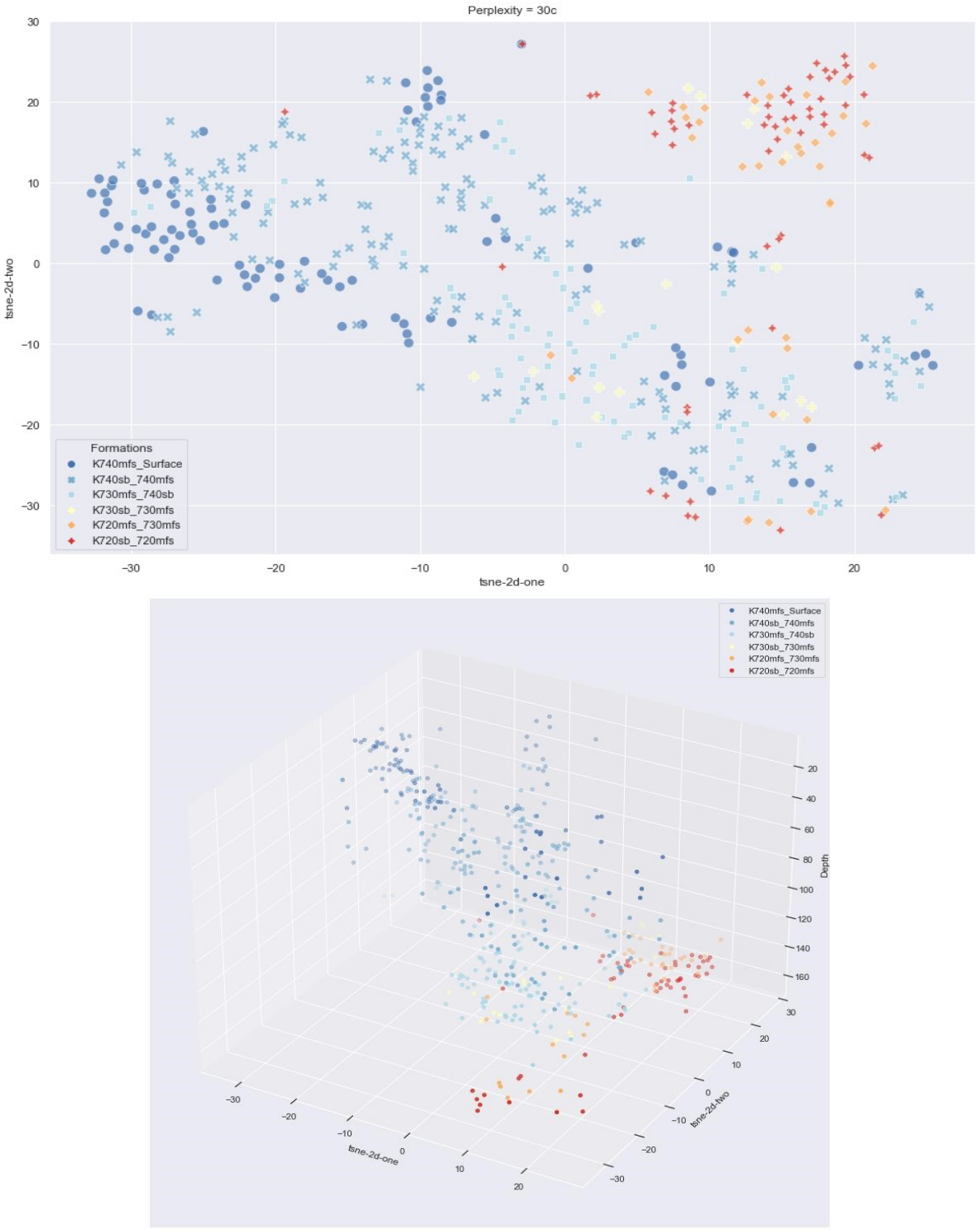

Figure 12: T-Distributed Stochastic Neighbor Embedding (t-SNE) of the GCA1 well in 2D (top) and 3D (bottom). The perplexity is 30 on both plots. Points are distinguished by shape and color, delineated by key sequence boundaries and maximum flooding surfaces within the Austin Chalk